thermo

MDPI

Article

Prediction of Performance and Geometrical Parameters of Single-Phase Ejectors Using Artificial Neural Networks

Mehdi Bencharif [1], Sergio Croquer [1], Yu Fang [1], Sébastien Poncet [1,*], Hakim Nesreddine [2] and Said Zid [3]

[1] Mechanical Engineering Departement, Université de Sherbrooke, Sherbrooke, QC J1K 2R1, Canada
[2] Laboratoire des Technologies de l'énergie, Hydro-Québec, Shawinigan, QC G9N 7N5, Canada
[3] Laboratoire de Génie Climatique Constantine-LGCC, Université Frères Mentouri Constantine 1, Ain Elbey, Constantine 25000, Algeria
* Correspondence: sebastien.poncet@usherbrooke.ca

Abstract: Ejectors have gained renewed interest in the last decades, especially in heat-driven refrigeration systems, to reduce the load of the compressor. Their performance is usually influenced by many factors, including the working fluid, operating conditions and basic geometrical parameters. Determining the relationships between these factors and accurately predicting ejector performance over a wide range of conditions remain challenging. The objective of this study is to develop fast and efficient models for the design and operation of ejectors using artificial neural networks. To this end, two models are built. The first one predicts the entrainment and limiting compression ratio given 12 input parameters, including the operating conditions and geometry. The second model predicts the optimal geometry given the desired performance and operating conditions. An experimental database of ejectors using five working fluids (R134a, R245fa, R141b, and R1234ze(E), R1233zd(E)) has been built for training and validation. The accuracy of the ANN models is assessed in terms of the linear coefficient of correlation (R) and the mean squared error (MSE). The obtained results after training for both cases show a maximum MSE of less than 10% and a regression coefficient (R) of, respectively, 0.99 and 0.96 when tested on new data. The two models have then a good generalization capacity and can be used for design purposes of future refrigeration systems.

Keywords: single-phase ejector; artificial neural network; ejector performance; ejector design; thermodynamic model

Citation: Bencharif, M.; Croquer, S.; Fang, Y.; Poncet, S.; Nesreddine, H.; Zid, S. Prediction of Performance and Geometric Parameters of Single-Phase Ejectors Using Artificial Neural Networks. *Thermo* **2023**, *3*, 1–20. https://doi.org/10.3390/thermo3010001

Academic Editor: Johan Jacquemin

Received: 23 November 2022
Revised: 16 December 2022
Accepted: 22 December 2022
Published: 28 December 2022

1. Introduction

Worldwide population growth and industrialization in developing countries have remarkably increased the demand for thermal comfort development during recent decades. The industry standard to meet this demand is the vapor compression refrigeration system (VCRS), which is known for its high capacity and ability to operate at cooling temperatures but also for its elevated energy requirements and relatively low energy performance. Many alternatives to the VCRS have been proposed in recent years with the main purpose of improving energy performance and reducing the use of refrigerant fluids. In this context, ejector-based refrigeration systems (ERS) have been proposed as a cost-effective and less pollutant alternative, most notably for moderate heating and cooling demands [1]. The heat-driven refrigeration cycle (HDRC) is a member of the ERS family where the mechanical compressor is replaced by three components: a pump, a generator, and a supersonic single-phase ejector, such that the latter acts as a thermo-mechanical compressor but without any moving parts. A general schematic of the HDRC is shown in Figure 1, along with the corresponding pressure–enthalpy diagram. In this cycle, high-pressure vapor (primary flow) is delivered from the generator. This flow enters the supersonic ejector and entrains the low-vapou-r pressure (secondary flow) coming from the evaporator. Both flows are mixed and compressed to an intermediate pressure throughout the ejector and the resulting

mixture is directed toward the condenser. The condensed liquid is split into two parts: one part is fed back into the pump and the generator, while the other is directed toward the throttling valve and the evaporator. The HDRC cycle has gained interest in recent years since it can be activated using waste heat or energy from renewable sources and allows the drop-in replacement of low global warming potential (GWP) refrigerants as working fluids at a low performance penalty [2].

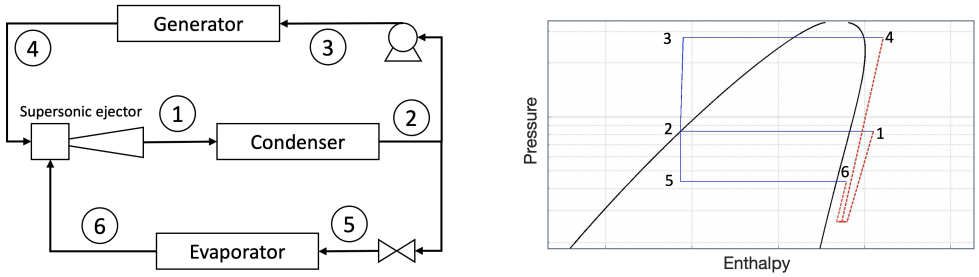

(**a**) (**b**)

Figure 1. (**a**) General schematics of the HDRC, along with (**b**) its corresponding pressure–enthalpy diagram.

The coefficient of performance (COP) of the HDRC is directly proportional to the entrainment ratio of the supersonic ejector [3]. The entrainment ratio, ω, is defined as the ratio between the secondary flow mass flow rate, $\dot{m}_s$, and the primary mass flow rate, $\dot{m}_p$. The other performance metric for a supersonic ejector is the compression ratio is P_{CR}, which is the ratio between the static pressure at the exit of the diffuser, P_{cond}, and the static pressure at the secondary flow inlet, P_{sec}. The typical supersonic ejector performance curve for fixed inlet conditions is displayed in Figure 2. Three operating modes can be distinguished as the outlet pressure increases: when ω does not change with P_{cond}, the ejector is said to be in a double-choked or on-design regime. This regime ends when the critical compression ratio or critical pressure $P_{crit,1}$ is reached. It marks the optimal operating point for a given geometry and inlet conditions. As P_{cond} augments beyond $P_{crit,1}$, the entrainment ratio decreases linearly P_{cond}. This is known as single-choke or off-design regime. Once the outlet pressure reaches the threshold $P_{crit,2}$, the ejector enters the malfunction mode, and back flow is observed at the secondary inlet.

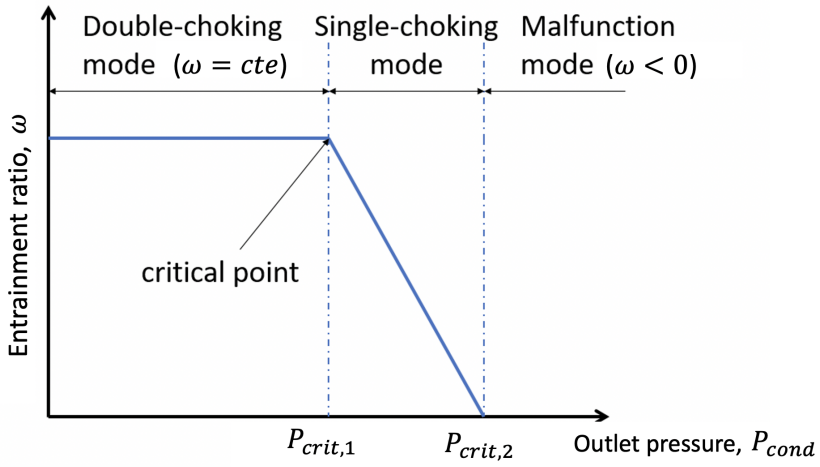

Figure 2. Operating modes of a supersonic ejector for a fixed geometry and given inlet conditions.

Figure 3 shows the basic geometry of a supersonic ejector along with the definition of the main geometrical parameters. After acceleration in the convergent–divergent nozzle, the primary flow entrains the secondary flow into the mixing chamber. Then, both flows interact in the constant area section until oblique shock waves take place before entering the

diffuser. Being the central component in ERS, the performance of supersonic ejectors has been thoroughly studied during the last decade for different configurations and working fluids. On the one hand, coupled interactions exist between the ejector performance metrics (ω and P_{CR}) and the system operating conditions [4], which affect both the steady operation and transients of the system [5]. On the other hand, experimental studies have shown the sensibility of the entrainment ratio to key geometrical parameters such as the area ratios relative to the nozzle throat area [6], the mixing chamber length [7,8] and the nozzle exit position (NXP) [9]. Similarly, the maximum possible compression ratio during double choke, P_{crit1}, has been linked to the diffuser outlet area and the NXP [10], the primary nozzle exit shape [11] and the design of the constant area section [12]. The interested reader is referred to Aidoun et al. [1] for a state-of-the-art description of ejector-based refrigeration cycles.

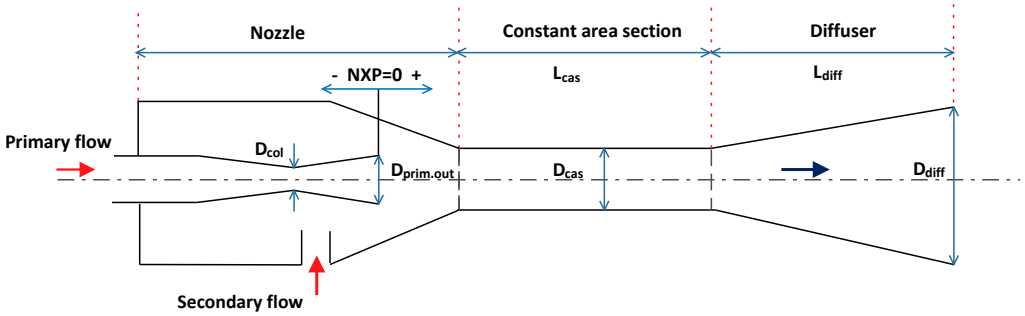

Figure 3. Schematic view of the ejector geometry.

Test benches for supersonic ejectors are often limited by construction costs, dimensions and operating conditions. Hence, design optimization and internal flow structure are often assessed using numerical tools. For instance, thermodynamic models, which take on the solution of conservation equations across specific ejector sections, allow quantifying the influence of different geometrical parameters on ejector [13,14] and cycle performance [15], as well as the integration with optimization algorithms [16]. Internal flow dynamics are better studied using computational fluid dynamics (CFD). These have permitted us to characterize the mean internal flow dynamics [17], quantify the relationships between internal phenomena and global performance [18,19] and trace the energy transfer mechanisms through the device [20]. However, in general, the computation and time requirements for CFD models are prohibitive for common industrial applications and extensive parametric studies.

Artificial neural network (ANN) is a field in artificial intelligence that mimics the behavior of the human brain to make predictions based on existing data. The power of ANN comes from its ability to learn directly from examples, tolerate relatively imprecise or incomplete data points and their lower vulnerability to outliers when compared to other machine learning approaches [21]. Moreover, ANN models are known as universal function predictors, i.e., they can be used to produce approximate solutions for complex non-linear systems, all without the need to know the underlying physics. Early efforts during the last decade have shown the potential of ANN to model and study the performance of ERS. For instance, Sözen and Akçayol [22] and Sözen and Arcaklioğlu [23] demonstrated the potential of shallow neural networks to optimize and determine the exergy losses of an ejector–absorption refrigeration cycle using the main temperatures as input parameters. Similarly, Wang et al. [24] showed that this type of ANN outperforms other machine learning approaches in the prediction of a hybrid ejector air-conditioning system.

Given their lower computational costs relative to CFD models, ANN models of supersonic ejectors are placed in an ideal position for integration with optimization algorithms, such as particle swarm optimization and ant colony optimization, to maximize cycle performance [25], as well as the construction of surrogate models to study the changes in internal flow properties [16]. Nonetheless, as it is still a relatively new tool, the proper application of ANN for ERS poses challenges requiring further study. To name a few: their generalization

capacity, input parameter selection, neural network architecture, best training algorithms, etc. In this regard, Gupta et al. [26] presented an ANN able to predict the entrainment ratio with a 90% accuracy and classify the operating regime (single- or double-choke) with a 91% accuracy when trained using an experimental database for different refrigerants. A novel contribution of their model is the inclusion of gas properties in the training database. In a follow-up study, these same authors showed that integrating two shallow neural networks, such that predictions of the first NN are fed into the second one, improved the prediction accuracy of entrainment ratio and operating regime to, respectively, 93% and ∼99% for a single-phase air ejector [27]. Similarly, Zhang et al. [28] determined that the Levenberg–Marquardt training algorithm showed better accuracy and performance over the resilient back-propagation and scaled conjugate gradient choices for predicting the back pressure of steam ejectors with condensation. Moreover, Zheng et al. [29] showed the feasibility of CFD results as training data for NNs meant for design optimization, even for two-phase ejectors.

The objective of this study is to provide greater insight into the use of ANNs for the study and optimization of supersonic ejectors by using this approach to establish relationships between ejector performance and the main governing parameters (geometry and operating conditions) as well as to provide tools for the design and operation of supersonic ejectors. To this end, two ANN models have been built using a dataset of 959 instances of experimental data collected from 22 studies on HDRC working with R134a, R245fa, R141b and R1234ze(E), R1234zd(E). The first model predicts the entrainment and compression ratio using 12 input parameters, including operating conditions and geometric characteristics. The second model estimates four geometry parameters, namely, the nozzle throat (D_{col}) and exit ($D_{prim,out}$) diameters, the nozzle exit position (NXP) and the constant area section diameter (D_{cas}) given the desired ω and P_{CR} and the temperatures and pressures at the inlets and the outlet. To the best of the authors' knowledge, this study is the most complete considering the number of different experimental databases used from various research groups (and so using different experimental set-ups) and types of refrigerant. Furthermore, for the first time, the full range of geometrical parameters and operating conditions and both performance metrics ω and P_{CR} are considered. Thus, the two ANN models can predict either the performance of the ejector based on its design or its design based on the targeted performance. Finally, the relative importance of all input parameters is quantified.

In the following section, the database and ANN construction steps are presented in detail. Results are then presented in Section 3, which includes model validation as well a discussion on the importance of the input parameters in both approaches. Finally, closing comments are given in Section 4.

2. Materials and Methods

2.1. Artificial Neural Networks

Artificial neural networks learn from input information and are able to process it for data classification, pattern recognition, finding approximation functions and simulating sophisticated operations [30]. Such a method is particularly well adapted to predict the properties of complex systems [31]. The architecture of an ANN is usually divided into three parts: an input layer, a hidden layer and an output layer. Each layer is composed of processing elements called perceptrons. These perceptrons receive input data from upstream elements, perform a weighted sum on it, transform the result using an activation function and output the result to the downstream layer. Original data are introduced into the input layer. During training, the input weights for each perceptron are adjusted by presenting the ANN with known data and minimizing its prediction error. This process is known as training. In this way, the ANN is able to establish its own relationships between the input and output parameters without any insight into the underlying physics.

ANNs synthesize and find correlations between inputs and outputs. Hence, sufficient and representative data are a must during the training process so the model is able to

recognize the underlying structure of the information involved. Otherwise, it risks being undertrained and is not able to find sufficiently accurate predictions on the training set. Once the ANN model is trained, its ability to make predictions on new data (a validation set) is tested by presenting it with new instances. Ideally, it will have the ability to predict outputs for any new input set of data within the range of the training data with an acceptable degree of accuracy. In summary, the process of any neural network-based model contains five main aspects [32]: (a) data acquisition, analysis, and problem representation; (b) determination of the network architecture; (c) determination for the learning process; (d) training; and (e) testing for generalization.

Different types of ANN exist depending on the mathematical operations and set of parameters required to determine the output. Some of the most used are multilayer perceptron (MLP) and radial basis function (RBF) [24]. Furthermore, there are different ANN training algorithms with varying learning speeds, stability and accuracy. One of the most popular is the back-propagation algorithm. It basically readjusts the weights for each perceptron to minimize the output error or cost function. The back-propagation training algorithm gradient descent with momentum is often too slow for practical problems because it requires small learning rates for stable learning. Faster algorithms such as conjugate gradient, quasi-Newton, and Levenberg–Marquardt use standard numerical optimization techniques [23]. These eliminate some of the disadvantages mentioned above. The latter (Levenberg–Marquardt) was used in this study.

In this study, the accuracy of the ANN models is evaluated in terms of mean squared error (MSE) and the regression correlation coefficient (R), which are defined below [33]:

$$MSE = \frac{1}{N}\sum_{i}|t_i - o_i|^2 \tag{1}$$

$$R = \sqrt{1 - \frac{\sum_i (t_i - o_i)^2}{\sum_i (o_i)^2}} \tag{2}$$

The mean squared error is the average squared difference between outputs and targets. Lower values are better. Regression R values are necessary to measure the correlation between the outputs and targets. R = 1 means a perfect correlation.

2.2. Database Description

The database was built by collecting experimental data points from the 22 references listed in Table 1. The references were chosen based on the number of details provided with regards to the geometry and working conditions. The collected data has been split into two parts: 800 instances (83.52%) are used for model building or training the dataset, and the remaining 159 instances (16.75%) are used as the final validation dataset. The model-building dataset (the 800 instances) was further split into a training set (70%), a validation set (15%) and a test set (15%). A randomized separation step was used to create the datasets, ensuring homogeneous distribution amongst all the groups. After division, the data were centered and normalized between -1 and $+1$ to make them consistent with the limits of a tangent sigmoid transfer function. The mean squared error and the linear coefficient of regression were used as cost functions. The references used for building the database were chosen using the following criteria:

- Only experimental data from HDRC, including single-phase ejectors, were collected;
- The working fluids are R134a, R245fa, R141b, R1234ze(E) and R1233zd(E). No mixture is considered.

Ejector performance is sensitive to the working fluid, the geometry and the operating conditions. Thus, the parameters for constructing the database were chosen accordingly in order to ensure proper representation of the ejector operation. As for the working fluid, four common refrigerants were chosen based on their popularity and the availability of

experimental references. The proportion of each working fluid in the database is: 37.53% R134a, 25.75% R245fa, 27.52% R141b and 9.17% for R1234ze(E) and R1233zd (E).

Table 1. Experimental studies on ejector refrigeration systems gathered for the construction of the database.

Working Fluid	Reference	Number of Data Points
R134a	Selvaraju and Mani [34] García del Valle et al. [12] Yan et al. [35] Li et al. [36] Poirier et al. [37] Falat et al. [38]	**360**
R245fa	Haghparast et al. [39,40] Hamzaoui et al. [5] Shestopalov et al. [41] Mazzelli and Milazzo [42] Scott et al. [43] Eames et al. [44,45] Narimani et al. [46] Bencharif et al. [47]	**247**
R141b	Huang et al. [14] Thongtip and Aphornratana [6,48] Ruangtrakoon and Thongtip [49]	**264**
R1234ze(E)-R1233zd(E)	Gagan et al. [50] Mahmoudian et al. [51]	**88**

The database parameters were split into three categories: geometrical parameters, operating parameters and performance parameters. These are summarized in Table 2, along with the numeric range and mean for each one. These allow us to assess the system's limits considered in this study. Since it is very difficult to find references that provide all the database parameters, some missing values were allowed in the experimental source. The proportion of missing values in the database for each parameter across all instances is also indicated in Table 2. It shows that the distribution of the parameters through the database is less than 4%. ANNs offer an advantage when some instances in the set are missing parameters since they can continue without any problems given their parallel nature. Using (RBF) interpolation is an advanced method in approximation theory for constructing high-order accurate interpolates of unstructured data [52].

Table 2. Range of inputs and outputs with their minimum, maximum and average values, as well as their distribution percentage.

Parameter	Units	Minimum	Maximum	Mean	Missing Values (%)
Geometrical Parameters					
Primary nozzle throat diameter (D_{col})	mm	0.50	20.20	5.68	0%
Primary nozzle outlet diameter ($D_{prim,out}$)	mm	0.80	26.32	9.13	0%
Nozzle exit position (NXP)	mm	0.00	69.93	18.55	0%
Constant area section diameter (D_{cas})	mm	0	34.07	10.46	0%
Constant area section length (L_{cas})	mm	0	223.77	69.21	4%
Diffuser oulet diameter (D_{out})	mm	2.60	108.30	34.91	4%
Diffuser length (L_{diff})	mm	11.50	950.00	212.39	4%

Table 2. *Cont.*

Parameter	Units	Minimum	Maximum	Mean	Missing Values (%)
Operating parameters					
Primary flow temperature (T_{prim})	°C	48	120	88.91	0%
Primary flow pressure (P_{prim})	kPa	400	3907.93	1514.13	0%
Secondary flow temperature (T_{sec})	°C	−7	30.60	9.98	0%
Secondary flow pressure (P_{sec})	kPa	20.50	630.00	195.72	0%
Condenser temperature (T_{cond})	°C	11.93	42.50	30.64	0%
Performance parameters					
Double-choke entrainment ratio (ω)	-	0.01	0.99	0.33	3.54%
Limiting compression ratio (P_{CR})	-	0.21	4.80	2.14	0%

2.3. Construction of the ANN Models

The main objective of the present work is the prediction of the performance parameters and geometric characteristics of an ejector for HDRC using four working fluids (R134a, R134a, R141b and R1234ze(E), R1233zd(E)). This is the first time the prediction of performance and geometric characteristics of different ejectors for a wide range of working fluids is estimated using ANN. It is also the first time both of these parameters are predicted using ANNs trained with more than one data source. Ejector performance is defined concerning the application of interest. The focus here is refrigeration and air conditioning, and entrainment and compression are the main parameters characterizing ejector operation. Two ANN models were constructed using the database parameters. These are summarized in Table 3. The first one is an operation model in which twelve input parameters (geometrical and operating parameters) are used to determine the ejector performance parameters (ω and P_{CR}). The second model is meant for design problems. In this case, the operating and performance parameters are used to determine the geometry parameters.

Table 3. Description of the input and output of the data for the two ANNs models.

ANN Model	Input Parameters	Output Parameters
Case 1: Ejector performance prediction	D_{col}, $D_{prim,out}$, NXP D_{cas}, L_{cas}, D_{out}, L_{diff} T_{prim}, P_{prim}, T_{sec}, P_{sec}, T_{cond}	ω, P_{CR}
Case 2: Geometry determination	ω, P_{CR}, T_{prim}, P_{prim} T_{sec}, P_{sec}, T_{cond}	D_{col}, $D_{prim,out}$, NXP, D_{cas}

The models were generated using the *MATLAB R2017b* neural network toolbox. A replica of the models was built in *IBM SPSS statistics 25* to verify their validity and to estimate the importance of the input parameters. They consist of an input layer, a single hidden layer and an output layer. The number of neurons in the hidden layer was determined using Equation (3) [53]:

$$n = \sqrt{n_i + n_o} + a \tag{3}$$

where n is the number of hidden layer neurons, n_i the number of neurons in the input layer, and n_o the number of neurons in the output layer. a is a fixed value ranging from 0 to 10. According to Equation (3), the number of neurons in the hidden layer ranges from 4 to 14 in Case 1 and from 3 to 13 in Case 2. In this study, the number of hidden layers is set to 10 neurons for both cases. This was determined using a trial and error approach. The resulting number of neurons is the minimum that provides a reasonable estimate of the output. Using more neurons leads to overfitting and poor generalization. For both models, the hyperbolic tangent sigmoid transfer function was used for the input and hidden layers. The neurons in the output layer used a linear transfer function.

In this study, a feed-forward back-propagation algorithm known as the gradient-descent method was used. This algorithm adjusts the weights automatically to minimize the error between the target values and the model output [54]. Other algorithms, such as the Levenberg–Marquardt, were used but they required more computational resources without any noticeable improvement in the results. Training automatically stopped once the ANN generalization stopped improving, as indicated by an increase in the mean square error of the validation samples.

Figure 4 illustrates the structure of the two ANN models. The circles represent the perceptrons and the arrows represent the unidirectional interconnections between them. Case 1 (Figure 4a) consists of 14 input neurons (D_{col}, $D_{prim,out}$, NXP, D_{cas}, L_{cas}, D_{out}, L_{diff}, T_{prim}, P_{prim}, T_{sec}, P_{sec}, T_{cond}) and 10 hidden neurons against two outputs neurons (ω) and (P_{CR}). In Case 2 (Figure 4b), the input layer consists of 7 neurons (ω, P_{CR}, T_{prim}, P_{prim}, T_{sec}, P_{sec}, T_{cond}) and 10 hidden neurons for 4 output neurons (D_{col}, $D_{prim,out}$, NXP, D_{cas}). The basic settings for both ANN models are summarized in Table 4.

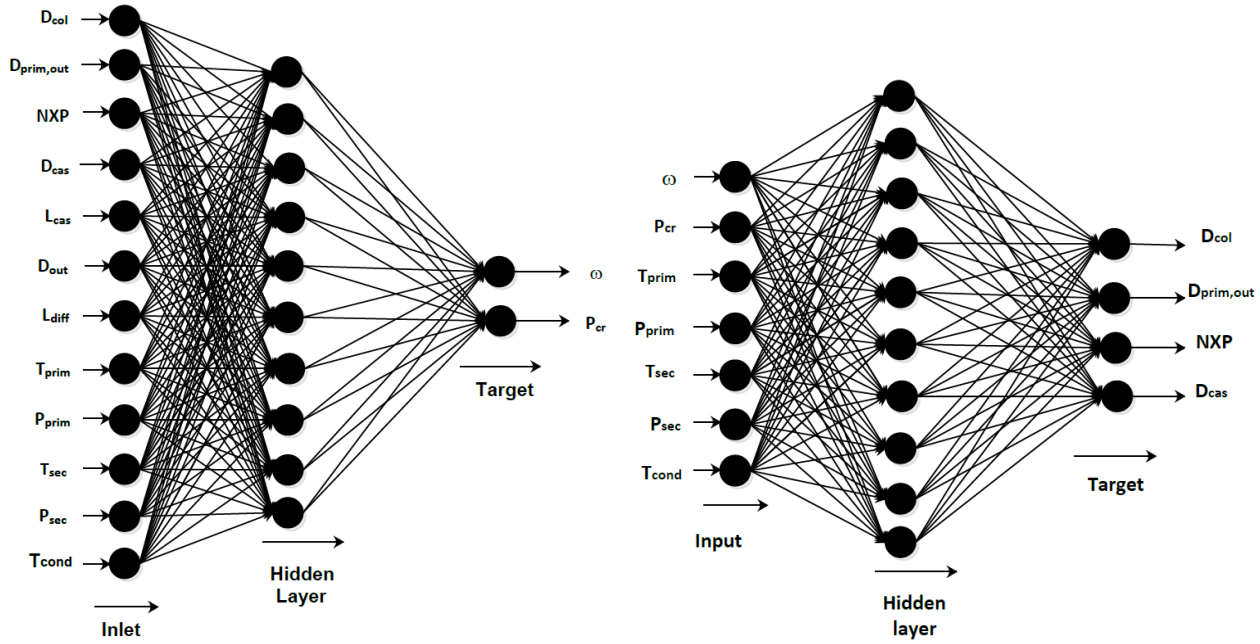

Figure 4. Structure of the ANN models for (**a**) Case 1 and (**b**) Case 2.

Table 4. Basic settings of the ANN models.

Parameters/Functions	Value
Algorithm	Levenberg–Marquardt
Transfer function	Tangent sigmoid
Performance parameters	Mean squared error
Number of hidden layers	10
Number of input layers	Case 1 (12) Case 2 (7)
Number of output layers	Case 1 (2) Case 2 (4)
Kinds of samples	Training 70 % , validation 15% and testing 15%
Train epoch	Dividerand

All the networks are trained, tested and validated using the Levenberg–Marquardt algorithm. As mentioned before, it is considered as one of the fastest algorithms [55] for training a neural network with a moderate size. The models include twelve input parameters for Case 1 and seven for Case 2 with 10 hidden layers for both networks. In terms of outputs, 2 parameters are predicted for Case 1 and 4 for Case 2, respectively.

Finally, the types of samples are as follows: 70% for training, and the remaining 30% is determined by the equality between the test and validation using a divider and training epochs.

2.4. Training

The performance of the ANN model depends on the success of the training process. During training, the model is presented with a set of labeled data (i.e., data for which the results are known) so it can iteratively adjust its weights in order to minimize the error between its predictions and the actual output values. Each iteration in the training process is also known as an epoch. Since at each epoch the weights are adjusted to the training set, there is a compromise between the number of epochs and the generalization capacity of the model. A successful training leads to accurate output predictions on the training, test and validation datasets.

2.5. Model Validation

The plot regressions shown in Figures 5 and 6 depict the ANN performance for the training, validation, and test datasets by comparing the model's predictions in both cases with the corresponding target values. The training step was repeated several times for both cases in order to obtain very high-accuracy models. Regarding Case 1 (Figure 5), a very good agreement is observed for each training set. Two point clusters can be recognized in each plot of Figure 5, one in the range of 0 to 1, corresponding to entrainment ratio predictions, and the other one in the range of 1.5 to 4, corresponding to the limiting compression ratio predictions. The correlation coefficient on the test set for this case ($R = 0.9685$) is very close to R for the training set (0.9609), which shows the model has a good generalization capacity. The highest differences between predictions and target values are observed for very low entrainment ratios, which usually correspond to single-choke operating ejectors. These conditions are much less represented in the database. Concerning Case 2 (Figure 6), a very good agreement is observed as well. The correlation coefficient on the test set in this case is $R = 0.9771$). The point clusters are harder to spot, given that there are four output parameters. The highest differences seem to take place close to zero, which corresponds to very small primary throat diameters as well as some missing values.

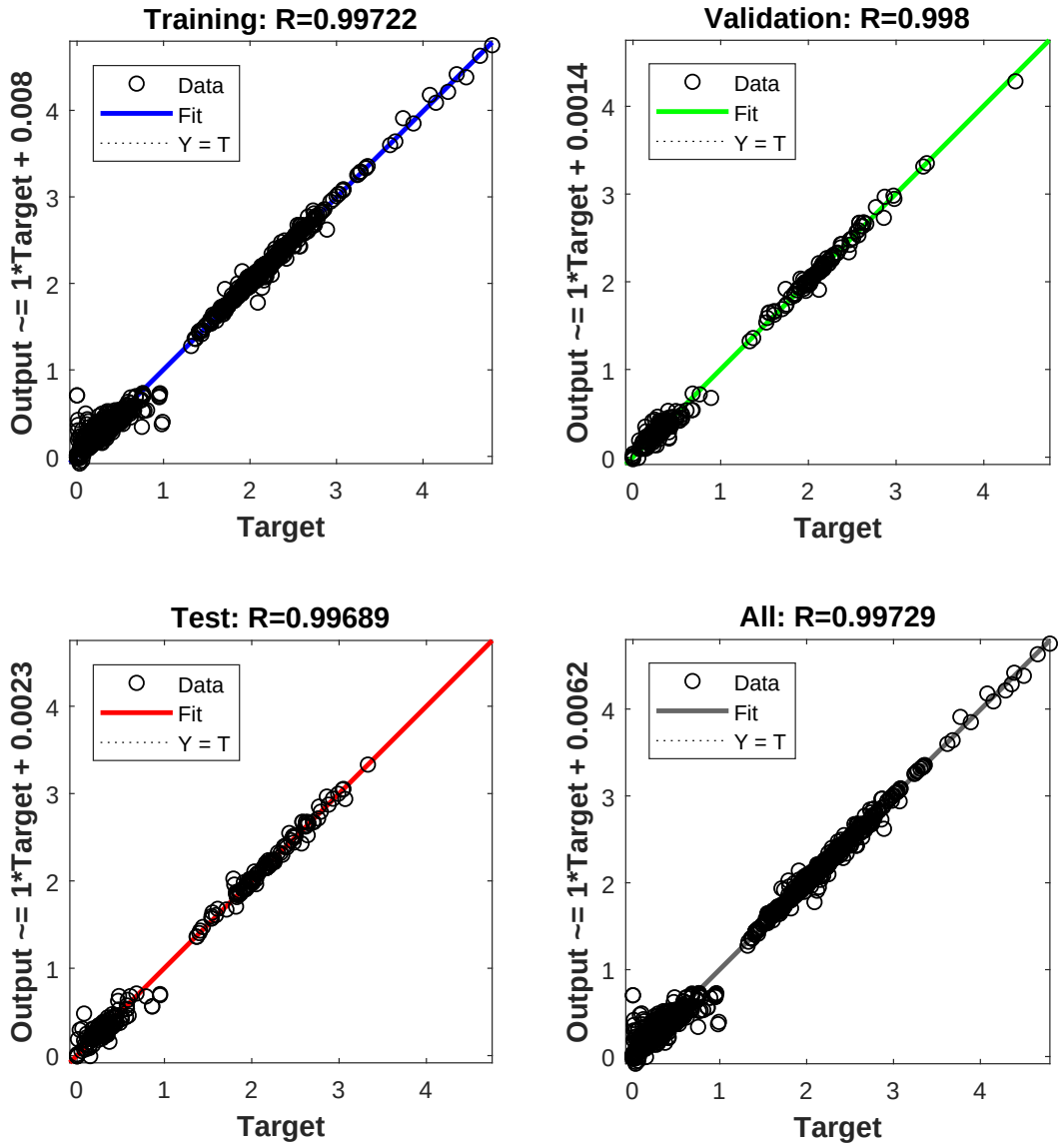

Figure 5. Comparison between the ANN predictions versus the target values (experimental data) for Case 1: prediction of ω and P_{CR}.

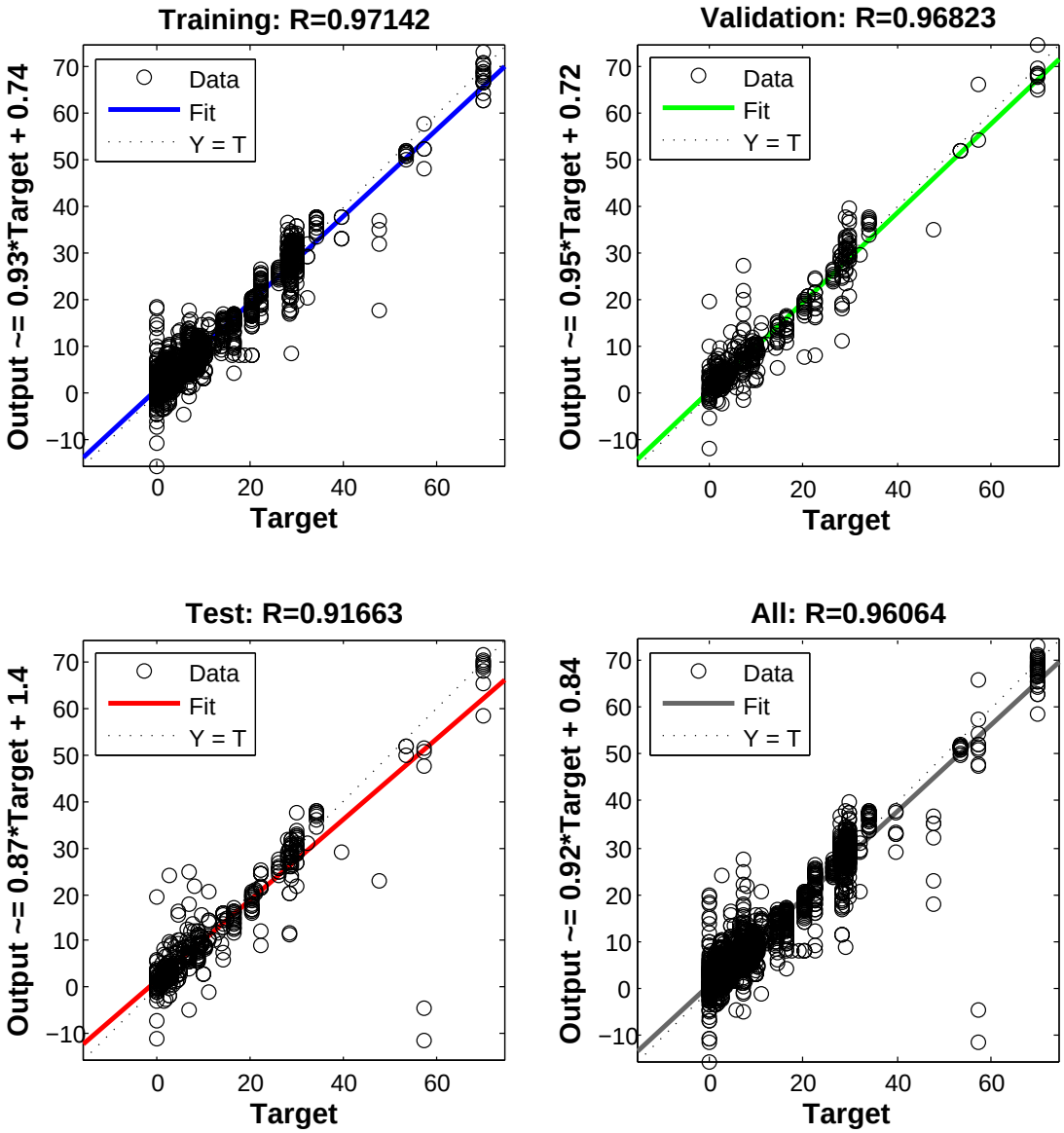

Figure 6. Comparison between the ANN predictions and the target values (experimental data) for Case 2: prediction of D_{col}, $D_{prim,out}$, NXP and D_{cas}.

3. Results

3.1. Generalization Capacity

The collected data include 959 data points divided into two groups: 83.25% were used in the training step, whereas the remaining 16.75% was used as blind data for further assessing the model's performance. Figure 7 compares the predictions versus target values (experimental data) for both models on the latter dataset. The correlation coefficients on this newly presented data are 0.9868 and 0.9262 for Cases 1 and 2, respectively. Regarding Case 1 (Figure 7a), the model shows good agreement in particular for entrainment ratio values of about 0 and 0.7 and limiting compression ratios between 1.5 and 3. There is a noticeable dispersion for target values $P_{CR} \geq 3$, which is related to the fewer data instances in this range. Furthermore, for Case 2, as shown in Figure 7b, there is an overall good agreement between ANN predictions and the target values concerning (D_{col}, $D_{prim,out}$, NXP and D_{cas}), although some dispersion is observed, in particular, for negative target values.

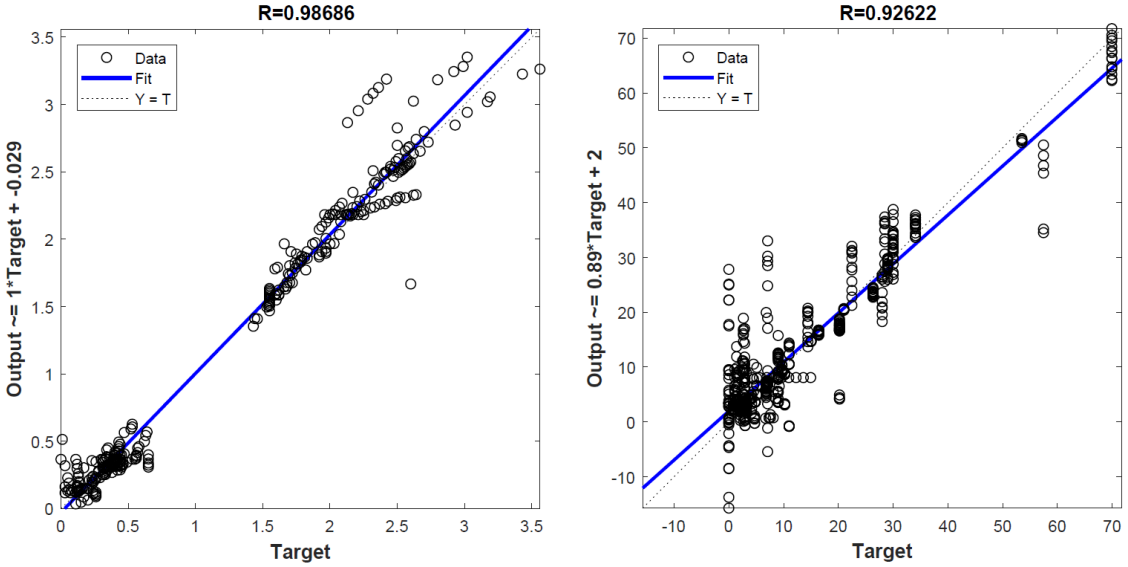

Figure 7. Comparison between the ANN predictions and the target values (experimental data) for the two models using the 159 data points from the database initially set aside: (**a**) Case 1 and (**b**) Case 2.

3.2. Operating Conditions

The ejector is particularly sensitive to its operating conditions, which is the correlation between the variation of the entrainment ratio (ratio between secondary and primary flow) and the backpressure (the backpressure is the pressure of the condenser), as shown in Figure 6. The ejector performance can be divided into three distinguished modes. The first one on the design or double choking-mode when both primary and secondary flow conditions are choked, as the flow pressure increases by further deceleration to equate the imposed backpressure, and ω is constant without any effect of the backpressure. The second one is off-design or single choking-mode, where only the primary flow is choked and the secondary flow is not; ω decreases while the back pressure increases above the critical value. The last mode is called back flow or reversed mode when both flows are not choked, and the back pressure exceeds the critical point, thus causing the reverse of the entrained flow. It results in negative ω values.

In this setting, the second set of the database comprising 159 sets of samples is used for a comparison between the results predicted by the ANN models (Cases 1 and 2), and the experimental data were carried out, including only the output data divided into two categories of on-design and off-design for both approaches. Figure 7 presents a set of results for ω and P_{CR} with critical and sub-critical conditions, and one can observe that a good agreement between ANN and experimental sets is achieved. However, the on-design mode (up) offers more accuracy compared to the off-design part (low). The entrainment ratio ω is located between (0.1 to 0.65) for the on-design section, while for the off-design section, there is more dispersion between (0 and 0.5) caused by the back pressure of the condenser P_{CR} is in the range of (1.5 and 2.6) regarding critical condition and between 1.5 and 3.3 relating to sub-critical position.

Figure 8 displays, for fixed geometrical parameters, the predicted values of the entrainment coefficient ω and the critical pressure P_{CR} for both on- and off-design conditions. The predictions remain quite good for P_{CR} and degrade a little bit between the on- and off-design conditions for ω. This behavior is expected due to the high sensitivity of the critical point relatively to the operating conditions and the sharp decrease of ω with P_{CR} in the off-design regime. Figure 9 presents the same kind of comparison for the three main geometrical parameters D_{col}, $D_{prim,out}$, and D_{cas} for Case 2. The accuracy of the ANN model remains quite acceptable and similar for the three parameters. The comparison

points out, in particular, a lack of experimental data to strengthen the prediction capability of the model.

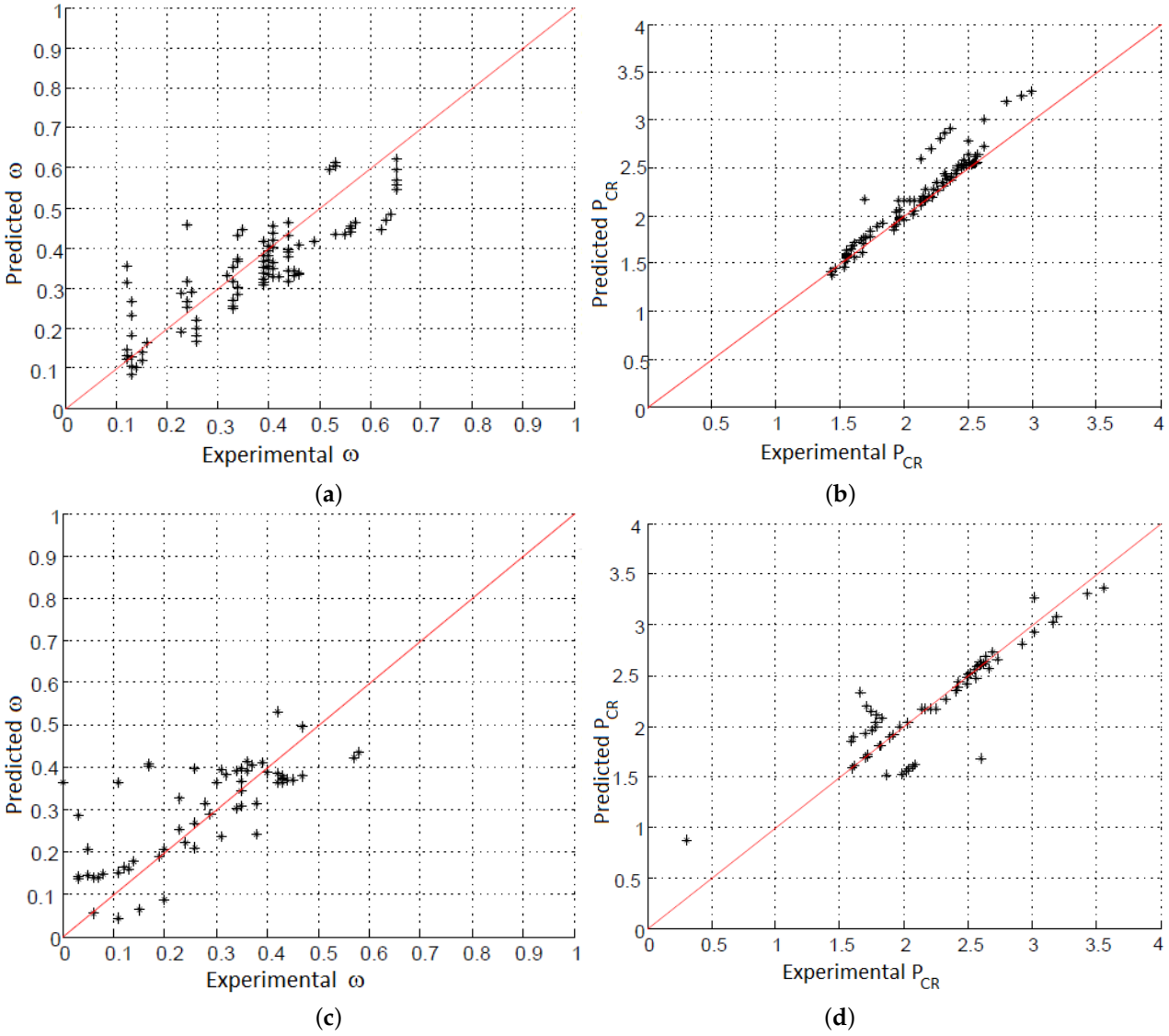

Figure 8. Comparison between the on-design (**a**,**b**) and off-design (**c**,**d**) modes in terms of ω (**a**,**c**) and P_{CR} (**b**,**d**).

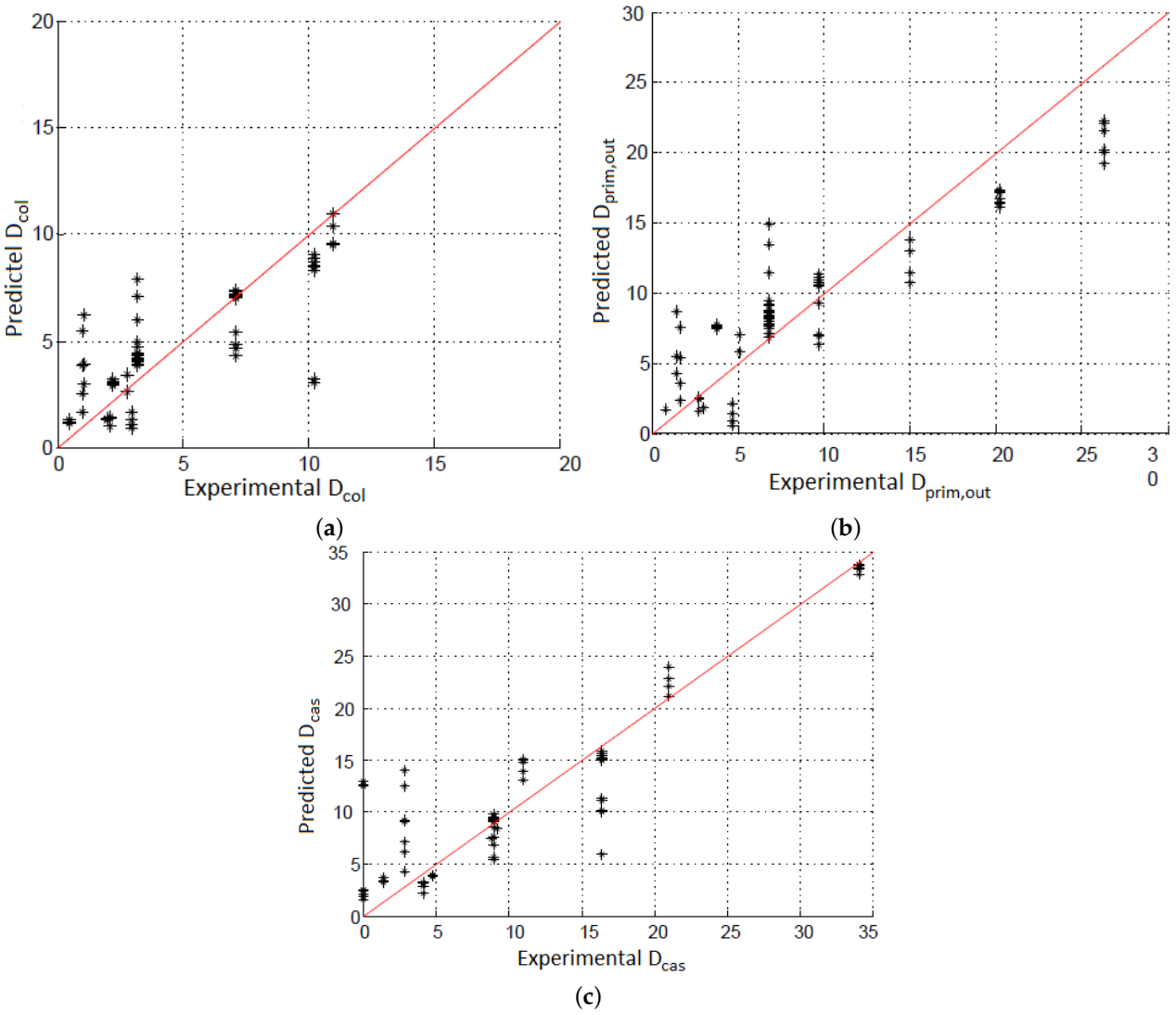

Figure 9. Predictions of the ANN model in terms of: (**a**) D_{col}, (**b**) $D_{prim,out}$, and (**c**) D_{cas} for Case 2.

3.3. Importance of Parameters

The ANN models for Cases 1 and 2 were built using, respectively, 12 and 7 input parameters for a set of data equal to 800. As shown in Section 3.1, these are able to accurately predict previously unpresented data, meaning they can be applied in new scenarios within the range of the training dataset. The models also allow estimating the importance of each input variable by assessing the change in the output variables when varying each feature at a time. This estimation was carried out using IBMSPSS on the two ANN models.

Figure 10 displays the importance of each input parameter (feature) on each model. The values are normalized using the most important feature as a reference. For an operation problem where the outlet parameters are ω and P_{CR} (Case 1), the operating conditions at the secondary inlet and the outlet (T_{cond}, P_{sec}) are the most influencing parameters ($\geq$80%). This is expected since the system's main control points are often the conditions at the condenser and the evaporator. The temperature and pressure of the secondary and primary flow followed by the diameters of primary nozzle conditions also have a higher importance level ($\geq$60%) but to a lesser extent. The less important parameters are the diameter and the length of the constant area section.

Concerning a design problem (Case 2), where the outlet parameters are the geometrical parameters: D_{col}, $D_{prim,out}$, NXP and D_{cas}, the most influencing features are the primary inlet conditions P_{prim} ($\sim$100%) and T_{prim} ($\sim$79%) followed by the secondary inlet conditions

(50%). It is also interesting to note that ω and P_{CR} are the least influencing parameters, despite being the objective of the model.

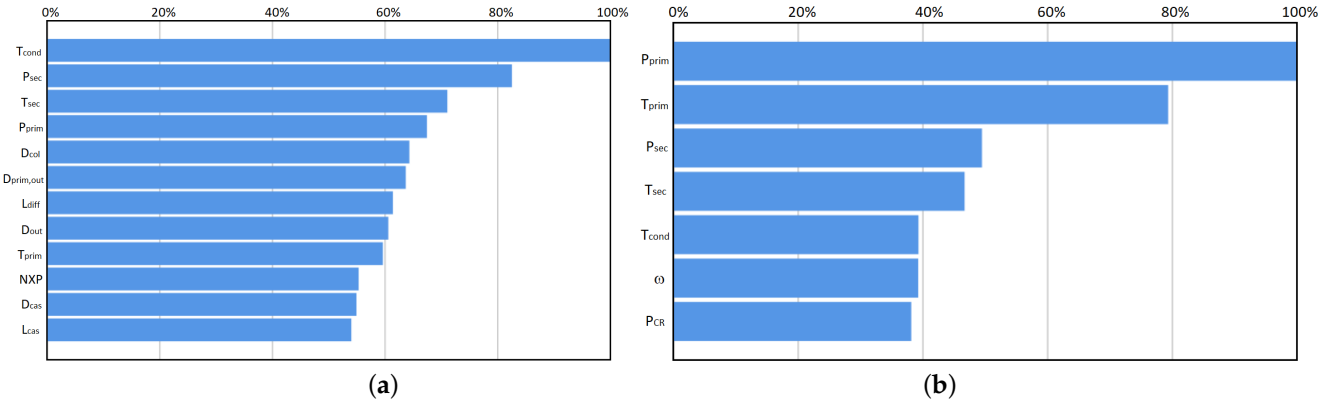

Figure 10. Relative importance of the input parameters on the model predictions for Cases (**a**) 1 and (**b**) 2.

As previously mentioned, studying the ANN models in depth allows for better comprehension. Another way to see the importance of the parameters is the use of scatterplot matrix, which is the collection of scatterplots organized into a grid or matrix. Each scatterplot shows the relationship between a pair of variables. Figures 11 and 12 display the operating parameters and geometrical characteristics, respectively, in terms of input parameters used to train, test, and validate two ANN models (Cases 1 and 2). Five (5) variables for operational conditions and seven (7) variables for geometrical characteristics are driven by 800 sets of data. In all cases, the optimal values fall in a range, where enough experimental data have already been collected.

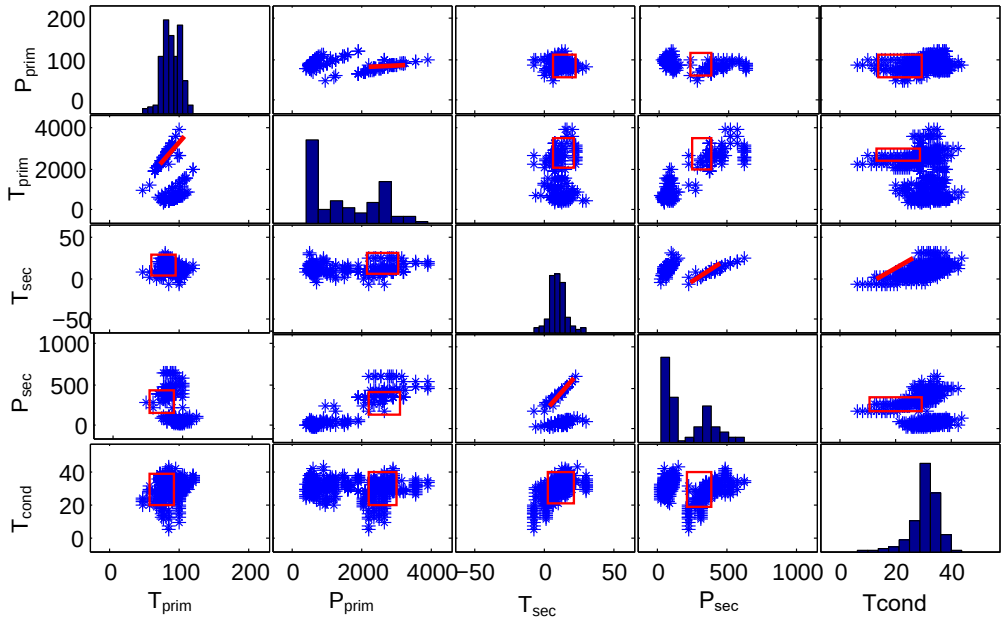

Figure 11. Scatter plot matrix of the input data regarding operating conditions. Rectangles and lines show the range of optimum parameters.

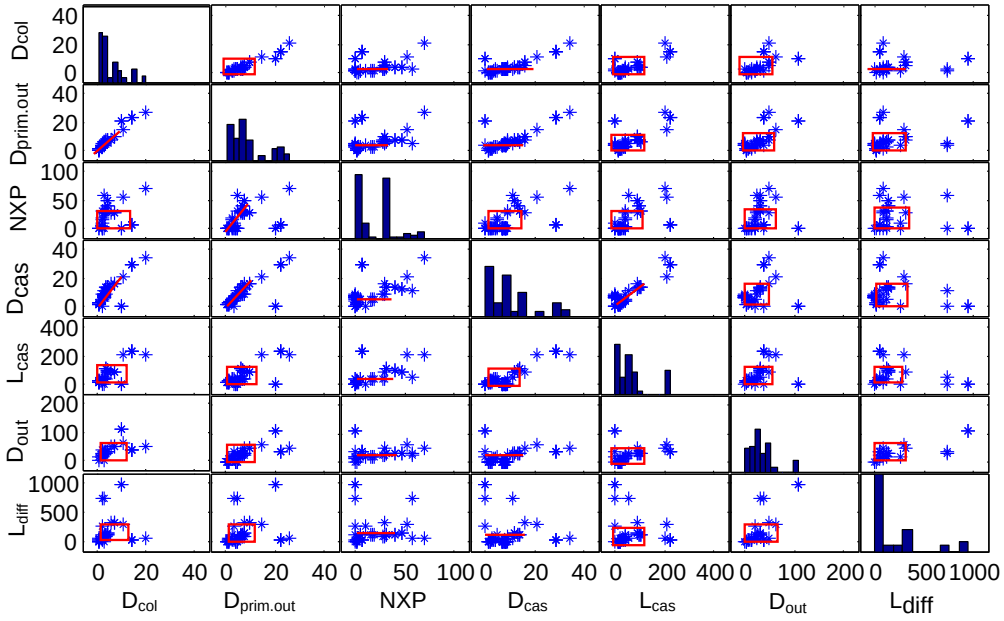

Figure 12. Scatter plot matrix of input data concerning geometric characteristics. Rectangles and lines show the range of optimum parameters.

The two ANN models developed in this investigation provide promising results. Another validation is proposed here for a single-phase supersonic ejector working with R245fa considered by Bencharif et al. [47]. Figure 13 confirms the validation of the proposed working mechanism of the first model. The predicted outputs are compared to experimental data, and the predictions of the thermodynamic model developed and validated by Croquer et al. [56] for an ejector-based HDRC working with R134a and later used and further validated by Bencharif et al. [47] for a R245fa ERS, both ejectors including droplet injection. A set of data is used to compare the three approaches, namely the experiments, the thermodynamic and ANN models. There is an overall fairly good agreement between the ANN results and the experimental data regarding the limiting compression ratio (Figure 13a) with an average relative deviation of less than $\varepsilon = 3\%$ and a maximum value of $\varepsilon = 26.5\%$. The ANN improves the predictions of the thermodynamic model. The average relative difference between the thermodynamic model and the experiments is indeed equal to $\varepsilon = 7.3\%$ (max. $\varepsilon = 30.7\%$).

Regarding the entrainment ratio (Figure 13b), the ANN predictions of ω follow the trends of the experimental data, although, at some points, it shows a greater deviation than the thermodynamic model and especially at lower condenser (ejector outlet) pressures. The average relative error between the ANN and the experiments remains quite acceptable: $\varepsilon = 16.5\%$, which decreases down to $\varepsilon = 10\%$ if one removes about 12% of the database, for which the experimental data may be close to the critical point but in the off-design regime. The relative error is similar between the thermodynamic model and the experiments. The maximum relative error ($\varepsilon = 80.1\%$) between the ANN and the experiments is reached at the maximum P_{out} considered here. As this ANN model only predicts the critical point on the operating curve, it may correspond, in fact, to a small deviation in P_{out} in comparison with the experiments for a given ω value.

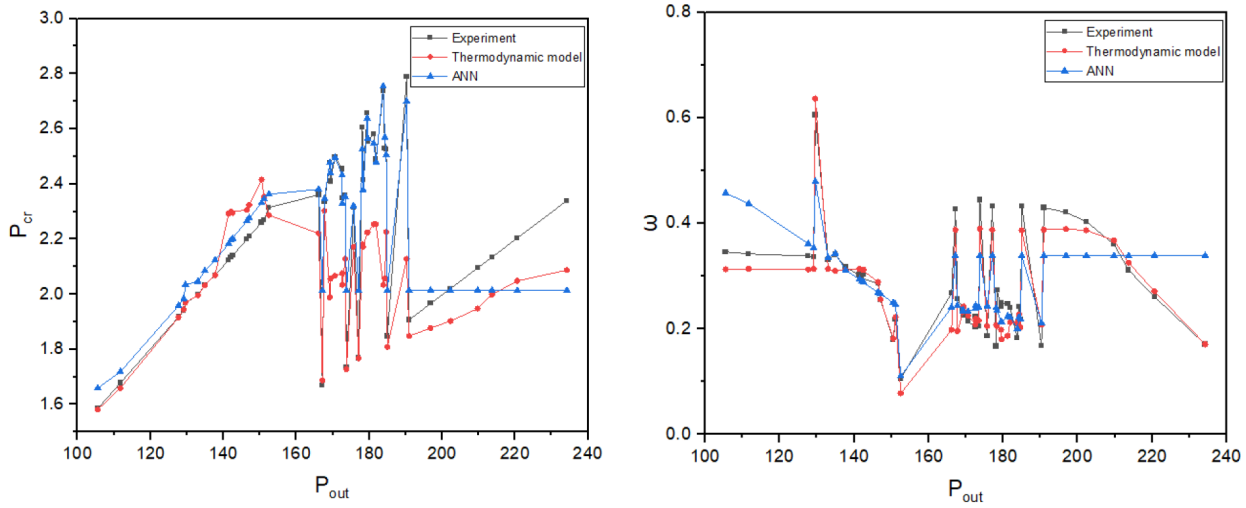

Figure 13. Comparison between the experimental data (□), thermodynamic (◇) and ANN (△) models in terms of (**a**) critical pressure P_{out} and (**b**) entrainment ratio ω. Results obtained for a single-phase supersonic ejector working with R245fa and considered by Bencharif et al. [47].

4. Conclusions

In this study, two ANN models have been constructed to predict the performance and main design parameters of supersonic ejectors for HDRC. The training database contained 800 data points of supersonic ejectors for HDRC with four working fluids: R141b, R134a, R245fa and R1234ze(E), R1233zd(E). The data were extracted from 22 different experimental references available in the literature. Furthermore, the models were validated and tested for generalization capacity using 159 additional data instances from these same sources. Two ANN models were constructed: Case 1, which predicts the ejector ω and P_{CR} given basic geometrical and operation parameters, and Case 2, which estimates geometrical parameters given the desired operating point and double-choke performance. Based on the results, the following conclusions can be drawn:

- Both approaches (Cases 1 and 2) show good accuracy. The maximum relative error for both models on the training set was less than 10%. Moreover, Case 1 absolute fractions of variance on the training and test dataset were, respectively, R = 0.9972 and R = 0.9968. For Case 2, the corresponding coefficients were, respectively, R = 0.9714 and R = 0.9166.
- When presented with a dataset of 159 new instances, models show absolute fractions of variance R = 0.9868 (Case 1) and R = 0.9262 (Case 2). This shows the high capacity of the models to predict newly presented data within their training range.
- Comparison between on-design and off-design with 159 data indicates that the two models agree very well with the experimental data. Otherwise, the critical mode offers better results than the sub-critical mode for both operating conditions and geometrical characteristics.
- The most important parameters in the prediction of the ejector performance are the operating conditions for the secondary inlet and outlet, followed by NXP and the primary inlet conditions. Whereas the primary and secondary inlet conditions are the most influential parameters for the estimation of geometrical parameters (D_{col}, $D_{prim,out}$, NXP and D_{cas}).
- Comparisons with experimental and numerical data show that the ANN can provide better accuracy over a wide range of data.

This study verifies the feasibility of using ANN models for predicting the performance and operation of ANN ejectors. Different from usual thermodynamic models, the ANN does not make any simplifications about the flow behavior and can be trained to cover a

wide range of working fluids, working conditions, and ejector dimensions. Nonetheless, constructing and preparing the database can be time-consuming and difficult to achieve for very specific situations. Further research in this area should be aimed toward a more efficient way of constructing the models and include more complex ejector configurations, such as two-phase ejectors, other ejector-based refrigeration cycles, and refrigeration cycle parameters, such as the COP and the cooling load.

Author Contributions: Conceptualization, M.B. and S.P.; Methodology, M.B., S.C., Y.F. and S.P.; Validation, M.B., S.C., Y.F. and S.P.; Formal analysis, M.B., S.C., S.P. and H.N.; Investigation, M.B., S.C. and Y.F.; Data curation, M.B.; Writing—original draft, M.B., S.C. and S.P.; Writing—review & editing, M.B., S.C., Y.F., S.P., H.N. and S.Z.; Supervision, S.P., H.N. and S.Z.; Funding acquisition, S.P. and H.N. All authors have read and agreed to the published version of the manuscript.

Funding: This research received no external funding.

Institutional Review Board Statement: Not applicable.

Informed Consent Statement: Not applicable.

Data Availability Statement: The data presented in this study are available on request from the corresponding author.

Acknowledgments: S.C., Y.F., and S.P. acknowledge the NSERC chair on industrial energy efficiency established at Université de Sherbrooke with the support of Hydro-Québec (laboratoire des technologies de l'énergie), Ressources Naturelles Canada (CanmetÉnergie) and Emerson Commercial and Residential Solutions.

Conflicts of Interest: The authors declare no conflict of interest.

References

1. Aidoun, Z.; Ameur, K.; Falsafioon, M.; Badache, M. Current Advances in Ejector Modeling, Experimentation and Applications for Refrigeration and Heat Pumps. Part 1: Single-Phase Ejectors. *Inventions* **2019**, *4*, 15. [CrossRef]
2. Chen, J.; Jarall, S.; Havtun, H.; Palm, B. A review on versatile ejector applications in refrigeration systems. *Renew. Sustain. Energy Rev.* **2015**, *49*, 67–90. [CrossRef]
3. Lawrence, N.; Elbel, S. Analysis of two-phase ejector performance metrics and comparison of R134a and CO_2 ejector performance. *Sci. Technol. Built Environ.* **2015**, *21*, 515–525. [CrossRef]
4. Chunnanond, K.; Aphornratana, S. An experimental investigation of a steam ejector refrigerator: The analysis of the pressure profile along the ejector. *Appl. Therm. Eng.* **2004**, *24*, 311–322. [CrossRef]
5. Hamzaoui, M.; Nesreddine, H.; Aidoun, Z.; Balistrou, M. Experimental study of a low grade heat driven ejector cooling system using the working fluid R245fa. *Int. J. Refrig.* **2018**, *86*, 388–400. [CrossRef]
6. Thongtip, T.; Aphornratana, S. An experimental analysis of the impact of primary nozzle geometries on the ejector performance used in R141b ejector refrigerator. *Appl. Therm. Eng.* **2017**, *110*, 89–101. [CrossRef]
7. Dong, J.; Hu, Q.; Yu, M.; Han, Z.; Cui, W.; Liang, D.; Ma, H.; Pan, X. Numerical investigation on the influence of mixing chamber length on steam ejector performance. *Appl. Therm. Eng.* **2020**, *174*, 115204. [CrossRef]
8. Rao, S.M.; Jagadeesh, G. Observations on the non-mixed length and unsteady shock motion in a two dimensional supersonic ejector. *Phys. Fluids* **2014**, *26*, 036103. [CrossRef]
9. Rand, C.P.; Croquer, S.; Poirier, M.; Poncet, S. Optimal nozzle exit position for a single-phase ejector (Experimental, numerical and thermodynamic modelling). *Int. J. Refrig.* **2022**, *144*, 108–117. [CrossRef]
10. Eames, I.; Wu, S.; Worall, M.; Aphornratana, S. An experimental investigation of steam ejectors for applications in jet-pump refrigerators powered by low-grade heat. *Proc. Inst. Mech. Eng. Part A J. Power Energy* **1999**, *213*, 351–361. [CrossRef]
11. Rao, S.M.; Jagadeesh, G. Novel supersonic nozzles for mixing enhancement in supersonic ejectors. *Appl. Therm. Eng.* **2014**, *71*, 62–71. [CrossRef]
12. García del Valle, J.; Saíz Jabardo, J.; Castro Ruiz, F.; San José Alonso, J. An experimental investigation of a R134a ejector refrigeration system. *Int. J. Refrig.* **2014**, *46*, 105–113. [CrossRef]
13. Galanis, N.; Sorin, M. Ejector design and performance prediction. *Int. J. Therm. Sci.* **2016**, *104*, 315–329. [CrossRef]
14. Huang, B.; Chang, J.; Wang, C.; Petrenko, V. A 1-D analysis of ejector performance. *Int. J. Refrig.* **1999**, *22*, 354–364. [CrossRef]
15. Bilir Sag, N.; Ersoy, H.; Hepbasli, A.; Halkaci, H. Energetic and exergetic comparison of basic and ejector expander refrigeration systems operating under the same external conditions and cooling capacities. *Energy Convers. Manag.* **2015**, *90*, 184–194. [CrossRef]
16. Ringstad, K.E.; Banasiak, K.; Ervik, Å.; Hafner, A. Machine learning and CFD for mapping and optimization of CO_2 ejectors. *Appl. Therm. Eng.* **2021**, *199*, 117604. [CrossRef]

17. Besagni, G.; Cristiani, N.; Croci, L.; Guédon, G.R.; Inzoli, F. Computational fluid-dynamics modelling of supersonic ejectors: Screening of modelling approaches, comprehensive validation and assessment of ejector component efficiencies. *Appl. Therm. Eng.* **2021**, *186*, 116431. [CrossRef]
18. Croquer, S.; Poncet, S.; Aidoun, Z. Turbulence modeling of a single-phase R134a supersonic ejector. Part 2: Local flow structure and exergy analysis. *Int. J. Refrig.* **2016**, *61*, 153–165. [CrossRef]
19. Croquer, S.; Lamberts, O.; Poncet, S.; Moreau, S.; Bartosiewicz, Y. Large Eddy Simulation of a supersonic air ejector. *Appl. Therm. Eng.* **2022**, *209*, 118177. [CrossRef]
20. Lamberts, O.; Chatelain, P.; Bartosiewicz, Y. New methods for analyzing transport phenomena in supersonic ejectors. *Int. J. Heat Fluid Flow* **2017**, *64*, 23–40. [CrossRef]
21. Haykin, S. *Neural Networks: A Comprehensive Foundation*; Prentice Hall PTR: Hoboken, NJ, USA, 1994.
22. Sözen, A.; Akçayol, M.A. Modelling (using artificial neural-networks) the performance parameters of a solar-driven ejector-absorption cycle. *Appl. Energy* **2004**, *79*, 309–325. [CrossRef]
23. Sözen, A.; Arcaklioğlu, E. Exergy analysis of an ejector-absorption heat transformer using artificial neural network approach. *Appl. Therm. Eng.* **2007**, *27*, 481–491. [CrossRef]
24. Wang, H.; Cai, W.; Wang, Y. Modeling of a hybrid ejector air conditioning system using artificial neural networks. *Energy Convers. Manag.* **2016**, *127*, 11–24. [CrossRef]
25. Rashidi, M.; Aghagoli, A.; Raoofi, R. Thermodynamic analysis of the ejector refrigeration cycle using the artificial neural network. *Energy* **2017**, *129*, 201–215. [CrossRef]
26. Gupta, P.; Kumar, P.; Rao, S.M. Artificial neural network model for single-phase real gas ejectors. *Appl. Therm. Eng.* **2022**, *201*, 117615. [CrossRef]
27. Gupta, P.; Kumar, P.; Rao, S.M. Artificial neural network based shape optimization of supersonic ejectors in the critical flow regime. *Appl. Therm. Eng.* **2022**, *216*, 119046. [CrossRef]
28. Zhang, K.; Zhang, Z.; Han, Y.; Gu, Y.; Qiu, Q.; Zhu, X. Artificial neural network modeling for steam ejector design. *Appl. Therm. Eng.* **2022**, *204*, 117939. [CrossRef]
29. Zheng, J.; Hou, Y.; Tian, Z.; Jiang, H.; Chen, W. Simulation Analysis of Ejector Optimization for High Mass Entrainment under the Influence of Multiple Structural Parameters. *Energies* **2022**, *15*, 7058. [CrossRef]
30. Haykin, S. Self-organizing maps. In *Neural Networks—A Comprehensive Foundation*, 2nd ed.; Prentice-Hall: Hoboken, NJ, USA, 1999.
31. Trabelsi, S.; Hafid, M.; Poncet, S.; Poirier, M.; Lacroix, M. Rheology of ethylene-and propylene-glycol ice slurries: Experiments and ANN model. *Int. J. Refrig.* **2017**, *82*, 447–460. [CrossRef]
32. Karami, H.; Ardeshir, A.; Saneie, M.; Salamatian, S.A. Prediction of time variation of scour depth around spur dikes using neural networks. *J. Hydroinform.* **2011**, *14*, 180–191. [CrossRef]
33. Akdag, U.; Komur, M.A.; Ozguc, A.F. Estimation of heat transfer in oscillating annular flow using artifical neural networks. *Adv. Eng. Softw.* **2009**, *40*, 864–870. [CrossRef]
34. Selvaraju, A.; Mani, A. Experimental investigation on R134a vapour ejector refrigeration system. *Int. J. Refrig.* **2006**, *29*, 1160–1166. [CrossRef]
35. Yan, J.; Chen, G.; Liu, C.; Tang, L.; Chen, Q. Experimental investigations on a R134a ejector applied in a refrigeration system. *Appl. Therm. Eng.* **2017**, *110*, 1061–1065. [CrossRef]
36. Li, F.; Li, R.; Li, X.; Tian, Q. Experimental investigation on a R134a ejector refrigeration system under overall modes. *Appl. Therm. Eng.* **2018**, *137*, 784–791. [CrossRef]
37. Poirier, M.; Giguère, D.; Sapoundjiev, H. Experimental parametric investigation of vapor ejector for refrigeration applications. *Energy* **2018**, *162*, 1287–1300. [CrossRef]
38. Falat, A.; Poirier, M.; Sorin, M.; Teyssedou, A. Experimental study of the performance of an ejector system using Freon 134a. *Exp. Therm. Fluid Sci.* **2019**, *105*, 165–180. [CrossRef]
39. Haghparast, P.; Sorin, M.V.; Nesreddine, H. Effects of component polytropic efficiencies on the dimensions of monophasic ejectors. *Energy Convers. Manag.* **2018**, *162*, 251–263. [CrossRef]
40. Haghparast, P.; Sorin, M.V.; Nesreddine, H. The impact of internal ejector working characteristics and geometry on the performance of a refrigeration cycle. *Energy* **2018**, *162*, 728–743. [CrossRef]
41. Shestopalov, K.; Huang, B.; Petrenko, V.; Volovyk, O. Investigation of an experimental ejector refrigeration machine operating with refrigerant R245fa at design and off-design working conditions. Part 2. Theoretical and experimental results. *Int. J. Refrig.* **2015**, *55*, 212–223. [CrossRef]
42. Mazzelli, F.; Milazzo, A. Performance analysis of a supersonic ejector cycle working with R245fa. *Int. J. Refrig.* **2015**, *49*, 79–92. [CrossRef]
43. Scott, D.; Aidoun, Z.; Ouzzane, M. An experimental investigation of an ejector for validating numerical simulations. *Int. J. Refrig.* **2011**, *34*, 1717–1723. [CrossRef]
44. Eames, I.W.; Ablwaifa, A.E.; Petrenko, V. Results of an experimental study of an advanced jet-pump refrigerator operating with R245fa. *Appl. Therm. Eng.* **2007**, *27*, 2833–2840. [CrossRef]
45. Eames, I.W.; Milazzo, A.; Paganini, D.; Livi, M. The design, manufacture and testing of a jet-pump chiller for air conditioning and industrial application. *Appl. Therm. Eng.* **2013**, *58*, 234–240. [CrossRef]

46. Narimani, E.; Sorin, M.; Micheau, P.; Nesreddine, H. Numerical and experimental investigation of the influence of generating pressure on the performance of a one-phase ejector installed within an R245fa refrigeration cycle. *Appl. Therm. Eng.* **2019**, *157*, 113654. [CrossRef]
47. Bencharif, M.; Nesreddine, H.; Croquer, S.; Poncet, S.; Zid, S. The benefit of droplet injection on the performance of an ejector refrigeration cycle working with R245fa. *Int. J. Refrig.* **2020**, *113*, 276–287. [CrossRef]
48. Thongtip, T.; Aphornratana, S. Development and performance of a heat driven R141b ejector air conditioner: Application in hot climate country. *Energy* **2018**, *160*, 556–572. [CrossRef]
49. Ruangtrakoon, N.; Thongtip, T. An experimental investigation to determine the optimal heat source temperature for R141b ejector operation in refrigeration cycle. *Appl. Therm. Eng.* **2020**, *170*, 114841. [CrossRef]
50. Gagan, J.; Śmierciew, K.; Butrymowicz, D. Performance of ejection refrigeration system operating with R-1234ze (E) driven by ultra-low grade heat source. *Int. J. Refrig.* **2018**, *88*, 458–471. [CrossRef]
51. Mahmoudian, J.; Mazzelli, F.; Rocchetti, A.; Milazzo, A. A heat-powered ejector chiller working with low-GWP fluid R1233zd(E) (Part2: Numerical analysis). *Int. J. Refrig.* **2021**, *121*, 216–227. [CrossRef]
52. Buhmann, M.; Dyn, N. Spectral convergence of multiquadric interpolation. *Proc. Edinb. Math. Soc.* **1993**, *36*, 319–333. [CrossRef]
53. Rafiq, M.; Bugmann, G.; Easterbrook, D. Neural network design for engineering applications. *Comput. Struct.* **2001**, *79*, 1541–1552. [CrossRef]
54. Kayabasi, E.; Ozturk, S.; Celik, E.; Kurt, H.; Arcaklioğlu, E. Prediction of nano etching parameters of silicon wafer for a better energy absorption with the aid of an artificial neural network. *Sol. Energy Mater. Sol. Cells* **2018**, *188*, 234–240. [CrossRef]
55. Mathworks, T. *Matlab Optimization Toolbox User's Guide*; MathWorks, Inc.: Natick, MA, USA, 2007.
56. Croquer, S.; Poncet, S.; Aidoun, Z. Thermodynamic modelling of supersonic gas ejector with droplets. *Entropy* **2017**, *19*, 579. [CrossRef]